J. Fluid Mech. (1999), *vol.* 378, *pp.* 71–96. Printed in the United Kingdom

An experimental investigation of screech noise generation

By J. PANDA

Modern Technologies Corporation, Middleburg Heights, OH 44130, USA
and NASA Lewis Research Center, Cleveland, OH 44135, USA
email: panda@yaz.lerc.nasa.gov

(Received 10 April 1996 and in revised form 17 March 1998)

The screech noise generation process from supersonic underexpanded jets, issuing from a sonic nozzle at pressure ratios of 2.4 and 3.3 (fully expanded Mach number, $M_j = 1.19$ and 1.42), was investigated experimentally. The extremely detailed data provide a fresh, new look at the screech generation mechanism. Spark schlieren visualization at different phases of the screech cycle clearly shows the convection of the organized turbulent structures over a train of shock waves. The potential pressure field (hydrodynamic fluctuations) associated with the organized structures is fairly intense and extends outside the shear layer. The time evolution of the near-field pressure fluctuations was obtained from phase-averaged microphone measurements. Phase-matched combined views of schlieren photographs and pressure fluctuations show the sound generation process. The individual compression and rarefaction parts of the sound waves are found to be generated from similar hydrodynamic fluctuations. A partial interference between the upstream-propagating sound waves and the downstream-propagating hydrodynamic waves is found to be present along the jet boundary. The partial interference manifests itself as a standing wave in the root-mean-square pressure fluctuation data. The standing wavelength is found to be close to, but somewhat different from, the shock spacing. An outcome of the interference is a curious ‘pause and go’ motion of the sound waves along the jet periphery. Interestingly, a length scale identical to the standing wavelength is found to be present inside the jet shear layer. The coherent fluctuations and the convective velocity of the organized vortices are found to be modulated periodically, and the periodicity is found to match with the standing wavelength distance rather than the shock spacing. The reason for the appearance of this additional length scale, different from the shock spacing, could not be explained. Nevertheless, it is demonstrated that an exact screech frequency formula can be derived from the simple standing wave relationship. The exact relationship shows that the correct spacing between the sources, for a point source model similar to that of Powell (1953), should be a standing wavelength (not the shock spacing).

1. Introduction

Screech noise is produced by incorrectly expanded supersonic jets issuing from nozzles of regular geometry. The characteristic discrete tones can be heard from over- and underexpanded supersonic jets. When present, the sound level associated with the screech tone dominates all other jet noise components in the forward direction (upstream of the nozzle exit, Tam 1991). Seiner, Manning & Ponton (1987) studied twin-jet screech resonance with nozzle geometries found in military aircraft and measured very high dynamic loads capable of causing tailplane structural failure. In an earlier study Hay & Rose (1970) also had made similar observations. This provides, in part, the motivation for the current work. The goal is to provide a knowledge base and a data base which can be used along with computational methods (Cain *et al.* 1995) to predict the frequency and amplitude of the screech tone.

The screech tone frequency can be predicted, but only approximately, using the existing formulae. The overall, self-sustaining, feedback loop that controls the screech production mechanism has been explained by Powell (1953 *a,b*). Since then there have been many visualization (Yu & Seiner 1983; Poldervaart, Vink & Wijnands 1968) and other experimental studies (Rice & Thagavi 1992; Norum & Seiner 1980; Westley & Woolley 1968, 1969, 1970; Brocher & Makhsud 1997) to validate the mechanism. The screech frequency formula proposed by Powell provides an approximation to the experimentally measured data. The next step in the buildup of the current understanding of screech was the establishment of a connection with the shock-associated broadband noise. Fisher & Morfey (1976) have demonstrated that Powell's (1953 *a*) relation can be obtained as a special case of the shock-associated broadband noise when the observation angle is at 180° with the flow direction. From an analysis of frequency spectra, Tam *et al.* (1986) have shown that the frequency spread of the broadband shock-associated noise decreases and the centre frequency approaches the screech frequency as the observation angle approaches 180°. The formulation proposed by Tam *et al.*, based on the above idea, once again provides only a reasonable approximation, instead of the correct prediction, of the screech frequency (Tam, Ahuja & Jones 1994). A correct description of the physics is expected to provide an accurate frequency prediction, which is absent in the previously published models. Another important, and still unsolved, part is the prediction of the screech tone amplitude, for which none of the above models provides an answer.

It is believed that the above inabilities are due to a gap in our understanding of many physical processes involved in the overall feedback loop. Some of the unresolved questions are the following. What is the exact nature of the feedback loop and where does it exist? Where do the effective sound sources exist? How do the shocks respond to a periodic train of disturbances and how do the sound waves generate more periodic disturbances in the flow (the receptivity problem)? An experimental program has been undertaken at NASA Lewis Research Center to answer some of the above questions. The present paper takes a fresh look into the details of the feedback loop, the sound generation process and the receptivity issue. A detailed study of the shock shapes and their motion in the plume of the same jets with identical operating conditions as in the present study has been presented earlier (Panda 1995 *a*, 1998).

Experimental data presented in this paper were obtained from either the jet shear layer or the extreme near-field region extending radially from just outside the shear layer to about seven diameters away from the centreline. The experimental techniques used for this study are non-intrusive in nature: microphone traverses outside the flow, laser light scattering by turbulence and schlieren visualization. Detailed phase-averaged measurements and schlieren photography were conducted to unveil the unsteady processes. The new observations are summarized in the last section: summary and conclusion.

Most of the earlier experimental work had concentrated on time-averaged measurements, while the sound generation process is a time-dependent one. A notable exception is a series of innovative experimental studies by Westley & Wooley (1968, 1969, 1970), who measured time-varying fluctuating pressures using analogue instru-

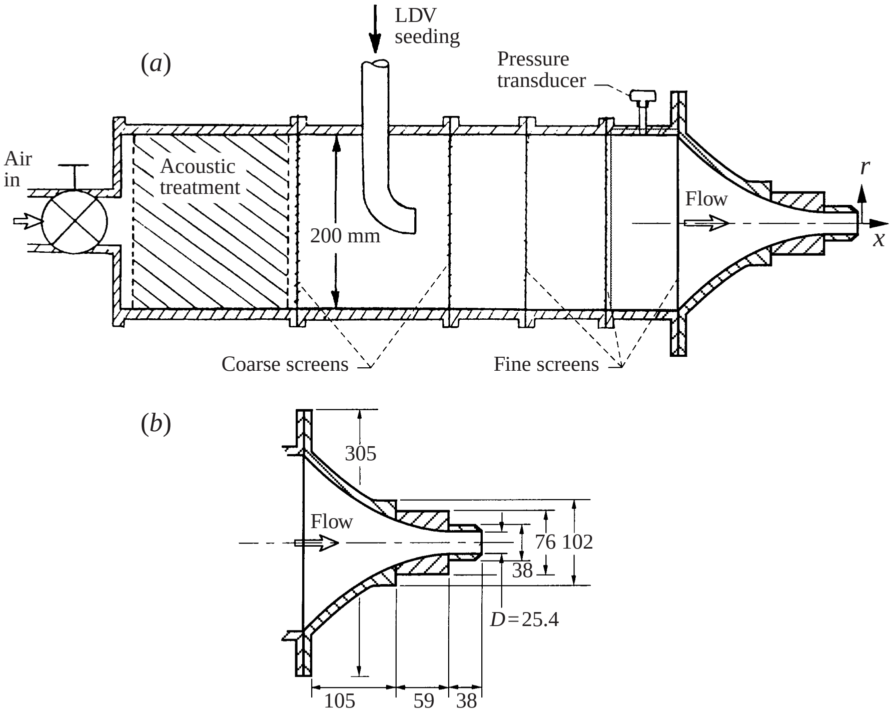

FIGURE 1. (*a*) Schematic of the jet facility. (*b*) Details of the nozzle block; all dimensions are in millimetres.

ments. Some observations made in these earlier studies have been duplicated in the present work, which makes extensive use of digital computers and analysers. The primary problem with the above studies is a limited phase resolution and a limited analysis of the experimental data. The limited phase resolution has obscured a significant amount of physics which is described in this paper.

2. Experimental set-up

The present experiments were conducted in a free air jet facility at the NASA Lewis Research Center (figure 1). A 25.4 mm diameter (D) axisymmetric, convergent nozzle was used to produce underexpanded supersonic jets which, if fully expanded, would have Mach numbers (M_j) in the range 1.1 to 1.65. The Mach number range was achieved by changing the supply pressure to the plenum chamber.

The experimental data reported herein were obtained using non-intrusive techniques. Since it is well-known that the screech is sensitive to the presence of any sound reflectors in the vicinity of the jet, all such objects, except for the nozzle flange, were wrapped in polyurethane foam to avoid strong reflection. Even when a probe or an optical element was placed close to the jet special attention was given not to changing the screech frequency. The primary reflector that has helped to produce a steady and a large-amplitude screech noise is the metallic nozzle block itself, detail of which is shown in figure 1 (*b*). The 305 mm diameter flange was found to be the major source of reflection. This was established by selectively covering individual surfaces with polyurethane foam. Both the screech amplitude and frequency can be changed by partly or fully covering the flange.

The screech tone frequencies and circumferential mode shapes have been measured for the above Mach number range and have been presented in an earlier publication (Panda 1995 *a*). The present experiments were conducted for two operating conditions, for which the fully expanded jet Mach numbers (M_j), screech frequencies and screech modes are respectively, 1.19, 8400 Hz, axisymmetric, and, 1.42, 5400 Hz, helical. The corresponding Reynolds numbers, based on the fully expanded jet velocity, U_j, and the nozzle diameter are, respectively, 0.93×10^6 and 1.26×10^6. The operating conditions were selected based on the availability of a stable screech tone. This is essential for an accurate phase-averaged measurement (Panda 1995 *a*, 1998).

The flow field was visualized by a standard schlieren system using two spherical mirrors, 152 mm in diameter and 914 mm in focal length. A spark source that provided enough light for about a microsecond duration was used to freeze the flow. The knife edge position is vertical; therefore, the horizontal density gradient is visible in all photographs presented in this paper. Light from the knife edge was allowed to fall directly on a Nikon F4 camera. The experiments were conducted in a dark room where the camera shutter was kept open and the light source was externally triggered to obtain a single image. The light source took several seconds to recharge before the next spark could be produced. To produce spark schlieren images at selected phases of the screech cycle a special triggering mechanism, composed of a delay generator and a single-pulse-capturing circuit, was built. The mechanism operated on a reference screech signal from a fixed microphone placed upstream of the nozzle exit. First, the reference signal was bandpass filtered around the screech frequency to eliminate all but the fundamental tone. The zero crossing points with positive slopes of the resulting sinusoidal wave were considered as phase references. The bandpassed reference signal was then fed to the adjustable delay generator that produced a series of pulses with the desired phase delay from the reference points. Since only one pulse was necessary to trigger the spark source (which would otherwise misfire) a single-pulse-capturing circuit was built. The physical operation involved selecting the desired phase delay in the delay generator and pressing a reset button on the single-pulse-capturing circuit to trigger the spark source. For phase-averaged photographs, the camera shutter was kept open and the film was exposed to six flashes produced with the same phase delay.

The convective speed of the organized turbulent structures was measured by an optical method involving a narrow pencil of laser beam passing through the shear layer and normal to the flow direction. The refractive index fluctuations associated with the density fluctuation of the passing eddies cause light scattering within a narrow angle with respect to the beam propagation direction (Truman 1992; Strohben 1978). This scattered light was collected and measured by a photo-multiplier tube (PMT).

The optical arrangement, shown in figure 2, is the same as used earlier to collect light scattered from shock waves (Panda 1995 *a*, *b*, 1998). A green (0.514 mm wavelength) laser beam, separated from an Argon-ion laser and transmitted through a fibre optic system, is the central element. The 2 mm diameter laser beam coming out of the fibre-optic probe is focused to a 0.16 mm spot at the jet centreline and is allowed to cross the flow field. On the other side of the jet is a light collecting and measuring device which senses the scattered light. A beam stop and an aperture stop are just in front of the 60 mm diameter collecting lens. The diameter of the beam stop is such that the main laser beam is blocked from entering the collecting optics while the scattered light can be easily collected. The collecting lens passes this light to a photomultiplier tube (PMT) via a pinhole. The electrical output from the PMT is connected across a 50 Ω terminator (not shown in figure 2). The voltage drop across

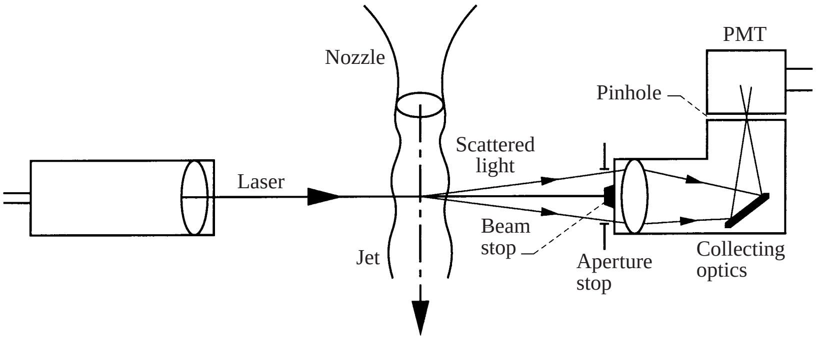

FIGURE 2. A schematic of the optical arrangement to detect laser light scattered by the jet flow.

the terminator is proportional to the PMT current and, therefore, is an indicator of the intensity of the collected light.

The complete optical set-up (fibre-optic probe, beam stop and the collecting optics) was mounted on a traversing unit (Klinger) which allowed it to be positioned at various points along the jet shear layer. Under no-flow condition light from the laser beam does not reach the PMT. However, when the flow is on the scattered light produced by the refractive index fluctuation in the flow is collected and sensed as a non-zero voltage output. It has been already mentioned that the same system was used to measure light scattered by shock waves present in the jet. However, the shocks are present at a few discrete regions, and the PMT signal level is nearly three orders of magnitude higher than that from the refractive index fluctuations alone. Therefore, it was straightforward to discriminate scattering signatures of organized structures from those of the shock waves. A voltage threshold level was established and PMT output above this level is considered due to light scattering by the shock. Data points indicating light scattering by shock waves are not presented in this paper. The voltage signal from the PMT, as well as all other voltage outputs from various measuring devices, were digitized using a dsp Technology sample-and-hold digital converter and then stored and processed by a Microvax 3300 computer.

The following points should be noted. The shock locations indicated in the figures correspond to their position in the jet shear layer. It has been pointed out in Panda (1998) that the shocks move most in the jet core and least in the shear layer. The second concerns the use of the term ‘jet boundary’. Strictly speaking, the radial boundary of the jet flow lies at infinity as the primary jet flow induces an entrainment motion in the ambient fluid. For the present work, however, jet boundary refers to the boundary of the turbulent motion from the primary jet, as visible in a schlieren photograph. It is estimated that, on average, the initial shear layer spreading is limited within a 5.7° angle with respect to the flow direction. A straight line drawn from the nozzle lip at the above angle is referred to the jet boundary in this paper.

3. Results

3.1. *Visualization of shock/organized structure interaction*

Figure 3 presents a set of 12 spark schlieren photographs over a screech cycle for the $M_j = 1.19$ jet. The constant value of phase difference between the successive photographs is 30° ($\Delta\tau/T = 0.083$, where τ is the phase time, and T is the time period of screech). Each photograph shows multiple dark regions corresponding to

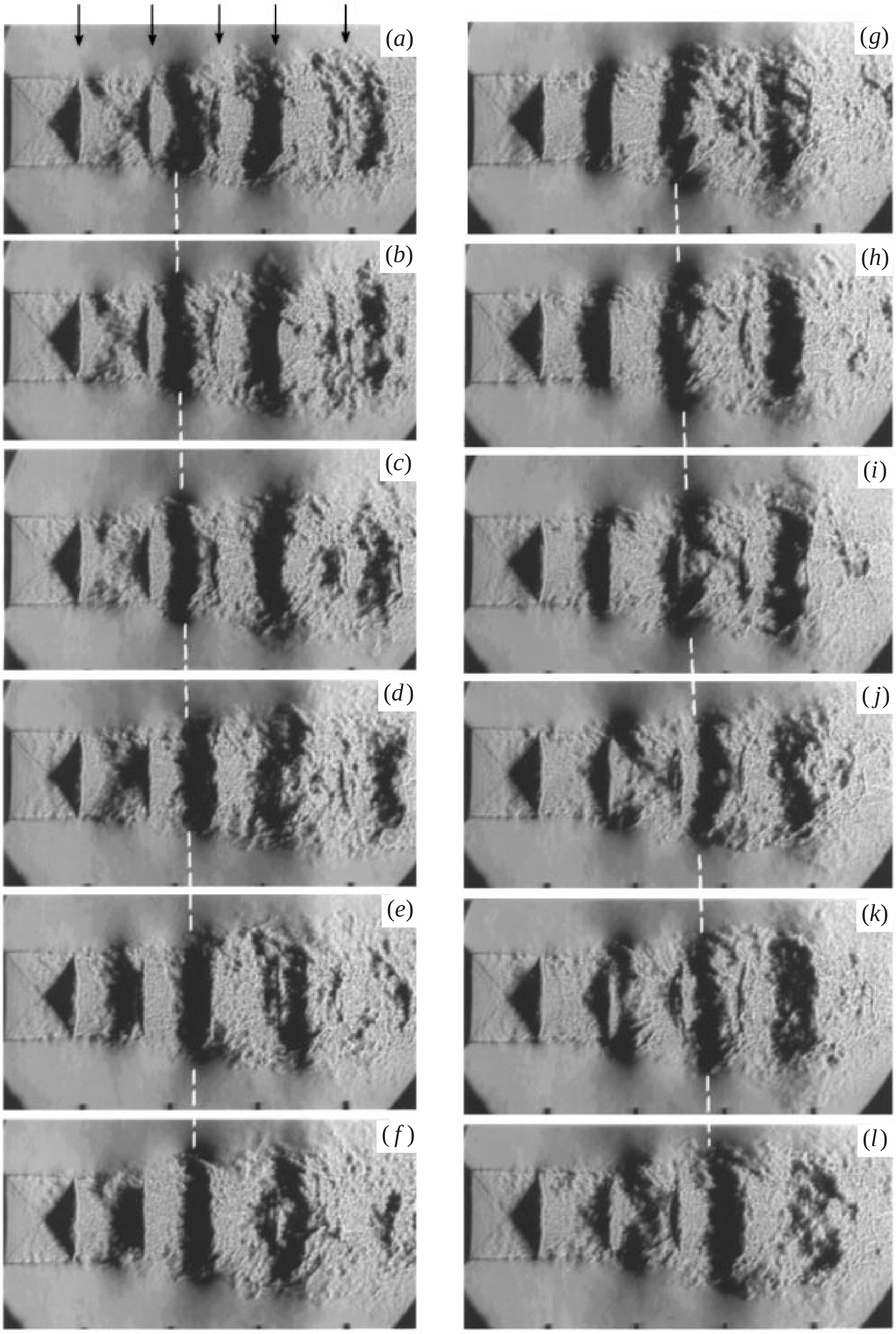

FIGURE 3. Spark schlieren visualization of $M_j = 1.19$ jet at 12 equi-spaced phases over a screech cycle. Vertical arrows in (*a*) indicate shocks. The chain line joins positions of one organized structure.

the high-density compression zones and, in between, lighter regions corresponding to the low-density expansion zones. An examination of the darker regions from frame to frame reveals two sets of periodic structures. One set is generally fixed in space and the other is convecting downstream. The fixed ones are the shock waves shown by vertical arrows in figure 3 (*a*), and the convecting ones correspond to the high-density sides of organized turbulent eddies. Perhaps the best way to discriminate between the two is by comparing the instantaneous photographs with a time-averaged photograph. The latter averages out signatures of the convecting structures and leaves the footprints of shocks. Such a time-averaged photograph is shown later. The vertical arrows in figure 3 (*a*), indicating shock boundaries in the jet shear layer, are obtained from such a comparison. In three dimensions the shock waves are imbedded in the jet core and have a conical or disk-like shape, while the organized turbulent structures are present in the jet periphery and are of doughnut shape. There are three to four axisymmetric organized structures in each photograph which are convecting over the shock train as the phase time progresses. The vertical and slightly inclined dashed line connects one such organized structure from frame to frame and portrays the convection process. The distance moved by each structure in a screech cycle is one wavelength (λ_h), which is also the spacing between two such consecutive structures in each photograph.

A noticeable feature is a considerable loss of coherence of the organized structures as they propagate beyond about four jet diameters (fifth shock) from the nozzle exit. The small markers at the bottom of each photograph are one jet diameter apart and a downstream distance of about five diameters is visible in each photograph. The organized structures are found to grow up to the second shock; they are most pronounced between the second and the fifth shock, after which they start to lose coherence.

It was estimated that there exists a random phase uncertainty of $\pm 15^\circ$ about the preset phase time in firing the spark unit. The phase time of the photographs in figure 3 is accurate within this uncertainty. In addition, there are certain other uncertainties inherent in a set of single-exposure images. There is a long time gap between the individual images, and the appearances of the organized structures are different from photograph to photograph due to their natural differences and jitter in position. Note that the shock waves also oscillate about their mean positions (Panda 1995 *a*, 1998). Such a motion, however, is difficult to see in figure 3.

3.1.1. *Phase-averaged schlieren photographs*

The jitter and cycle-to-cycle difference in the schlieren photographs of figure 3 are somewhat averaged out in the multiple-exposure (six) phase-averaged photographs of figure 4. Note that figure 4 shows the $M_j = 1.42$ jet which produces screech in a helical mode, while figure 3 corresponds to the $M_j = 1.19$ jet where screech tone is in an axisymmetric mode. The helical screech mode implies that the organized turbulent structures also have the same helical azimuthal shape. This is discernible at the right-hand edge of the photographs. The axisymmetric shock waves are distinctly separable from the organized structures. Another major difference is produced by a larger knife-edge cutoff that makes a more sensitive schlieren arrangement. The higher schlieren sensitivity has accentuated an additional feature: the near-field pressure fluctuation outside the jet flow boundary. Schlieren photographs of Yu & Seiner (1983) also shows this feature, albeit at a limited phase intervals.

The jet flow field is marked by a plethora of tiny bright and dark grains left by the random turbulent fluctuations. The darker, higher-density sides of the organized structures are found to extend beyond the jet boundary into the very near-field

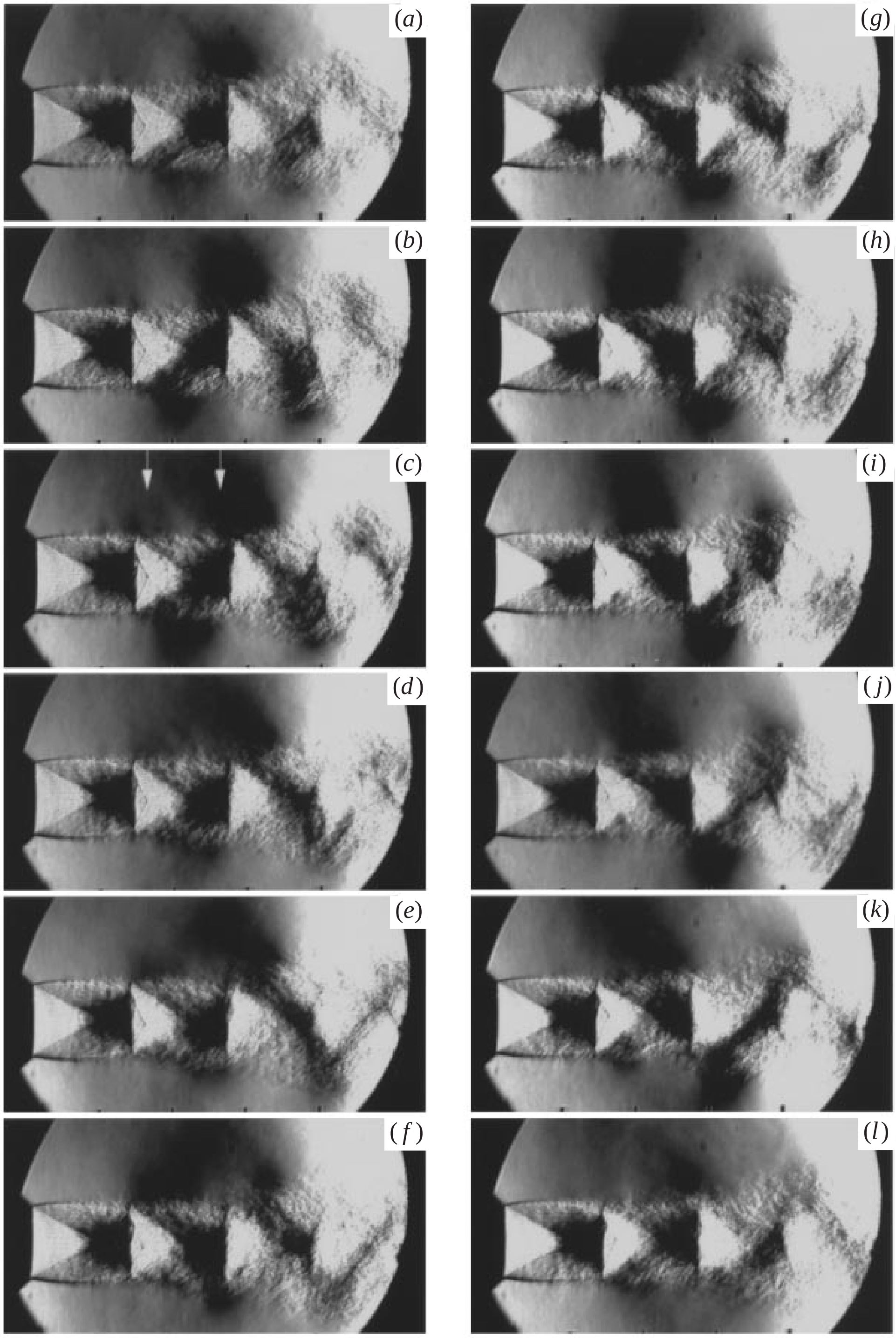

FIGURE 4. Phase-averaged schlieren photographs of $M_j = 1.42$ jet at 12 equi-spaced phases over a screech cycle.

region. These are the footprints of compression zones associated with hydrodynamic and acoustic waves. One problem with the phase-averaged photographs is a loss of sensitivity at the right-hand edge, which prohibits visualization of the near-field pressure fluctuations beyond about three jet diameters. The large knife-edge cutoff has accentuated the small optical coma at the second focal point of the schlieren setup and is believed to be the reason for the non-uniformity.

In spite of the above problem a curious merging process between two adjacent compression waves becomes apparent in figure 4(*c*–*g*). A weak (upstream) and a strong (downstream) compression zone at the top half of the jet in figure 4(*c*) (indicated by two vertical arrows) are found to go through a merging process that ultimately resulted in an exchange of energy, whereby the upstream zone becomes stronger. It will be shown later in the paper that this is the process by which the downstream-propagating hydrodynamic field interacts with the upstream-propagating acoustic waves.

3.2. *Time-averaged data*

Figure 5 shows schlieren photographs of the jets and the r.m.s. value of the fluctuating pressure measured in the near field using a traversing microphone. Each schlieren photograph was obtained by exposing a single negative to eight random flashes which, in effect, produced a time-averaged view of the flow field. The darker regions represent shock compression and the brighter ones expansion zones. The sharp vertical boundary at the end of each compression zone corresponds to the termination position of each shock in the shear layer around the jet.

The root-mean-square of the fluctuating pressure at the screech frequency, expressed in the standard decibel scale (reference level = 2×10^{-5} Pa), was obtained from narrow-band frequency spectra. The spectral levels at the screech frequency are plotted in this figure. The 3.18 mm microphone was traversed from point to point over a grid of 53 axial by 19 radial positions for the $M_j = 1.42$ case, and 51 axial by 21 radial for the $M_j = 1.19$ case. The grid spacing is uniform in the axial direction ($0.15D$ for $M_j = 1.42$ and $0.12D$ for $M_j = 1.19$ jets) and is progressively increased from $0.2D$ to $0.4D$ in the radial direction. This provided about 16 (closest to the jet boundary) to five (farthest from the boundary) points per acoustic wavelength, which is deemed to be sufficient to resolve the pressure fluctuations. To avoid damaging the fragile microphone diaphragm from direct impingement of the jet flow, traverses were made outside the flow boundary. The 5.7° angle with respect to the jet axis, visible at the lower edge of each colour plot, was chosen to account for the jet spread in the downstream direction. The fluctuating pressure levels shown in these plots have contributions from the acoustic waves radiated by the jet as well as from the hydrodynamic pressure field of the passing organized structures in the shear layer. This will be especially clear from the later discussion.

The time-averaged fluctuating pressure field is quite complex. The overall appearance, however, is similar for the two cases presented in this figure. There are two sets of periodic patterns visible in each colour plot: the red-yellow pattern along the jet boundary, and the red-blue pattern along a diagonal. The axisymmetric nature of the flow field implies that in three dimensions the patterns are wrapped around the jet. Similar experimental data and periodic patterns were also presented by Westley & Wooley (1968, 1969) for an axisymmetric jet and Rice & Taghavi (1992) for a rectangular jet. The red-yellow pattern along the jet boundary is considered first. The r.m.s. value of the pressure fluctuations differ by 20 dB between the yellow (crest) and red (trough) regions. A comparison with the schlieren photographs shows that

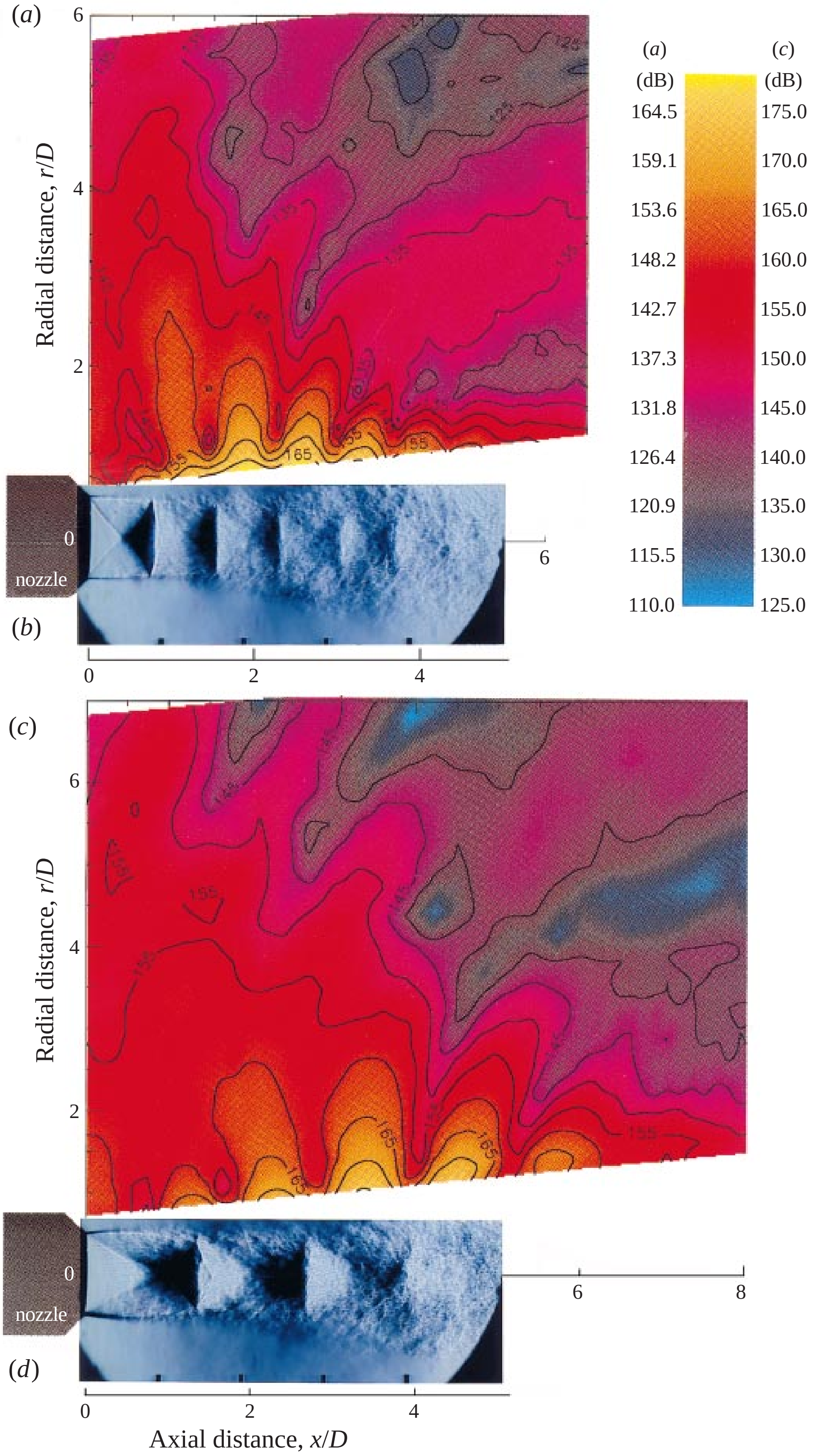

FIGURE 5. RMS pressure fluctuations at screech frequency and schlieren photograph for (*a*), (*b*) $M_j = 1.19$ and (*c*), (*d*) 1.42 jets. The superimposed contour levels are at 5 dB intervals.

M_j	Av. spacing between pressure crests (L_p/D)	Wavelength, acoustic (λ_s/D)	Wavelength, hydrodynamic (λ_h/D)	Standing wavelength (L_{sw}/D)	Average shock spacing (L/D)
1.19	0.67	1.59	1.15	0.66	0.77
1.42	1.02	2.49	1.74	1.03	1.28

TABLE 1. Length scales relevant to the near-field pattern along jet boundary

there is a small mismatch between the shock spacing (L) and the spacing between the crests (L_p). In general, crests lie between two adjacent shock tips. There are, however, visible exceptions; the pressure crest just over the first shock in figure 5 (*c*) being an example.

From an examination of the various wavelengths involved, it can be shown that the maxima and the minima in the pressure fluctuations are due to standing wave formation between the downstream-propagating hydrodynamic and the upstream-propagating acoustic fluctuations. The frequency of the hydrodynamic fluctuations is known to be the same as that of the emitted screech tone (Hu & McLaughlin 1990; Raman & Rice 1994). This is also confirmed from the shear layer turbulent fluctuation measurement. The wavelengths of hydrodynamic pressure fluctuation are measured from the phase-averaged data presented later in the paper. If we consider two oppositely moving wave systems of the same frequency, ω, different wavenumbers k_s and k_h, and different amplitudes A and B, the resultant pressure fluctuation can be written as

$$R = A\sin(k_s x + \omega t) + B\sin(k_h x - \omega t). \tag{1}$$

The mean-square of the resultant fluctuation is calculated as

$$\bar{R}^2 = \frac{\omega}{2\pi}\int_0^{2\pi/\omega} R^2\,\mathrm{d}t = \frac{A^2}{2} + \frac{B^2}{2} - AB\cos(k_s + k_h)x.$$

The above equation shows that a standing wave pattern is expected with a resultant wavenumber $k_{sw} = k_s + k_h$. If k_h is associated with the hydrodynamic fluctuations of wavelength λ_h ($k_h = 2\pi/\lambda_h$), k_s with the sound waves of wavelength λ_s, and k_{sw} with the standing waves of wavelength L_{sw}, then

$$\frac{1}{L_{sw}} = \frac{1}{\lambda_s} + \frac{1}{\lambda_h}. \tag{2}$$

Table 1 demonstrates that the spacing between neighbouring crests (L_p) follows the (2), i.e. $L_p = L_{sw}$. In the past, Davis & Oldfield (1962), Westley & Wooley (1968), Rice & Taghavi (1992), and Tam (1991) have qualitatively attributed the crest and troughs to a standing wave formation. It should be mentioned here that only a partial standing wave formation is expected as the amplitudes A and B are unequal. Along the jet boundary, the hydrodynamic fluctuations are found to be an order of magnitude higher than the acoustic fluctuations. However, the hydrodynamic fluctuations decay exponentially away from the jet boundary (Dahl 1994; Morris 1977), which makes the acoustic fluctuations dominate after a certain radial distance.

A second system of standing waves is expected due to the presence of a large flange upstream of the nozzle exit (figure 1). Interference between the incident and the reflected acoustic waves from the flange surface is expected to produce this system, which perhaps is manifested as the red-blue diagonal pattern in figure 5. The present paper does not analyse this standing wave system which, however, has been discussed recently, by Raman, Panda & Zaman (1997).

3.2.1. *Screech frequency formulation based on the standing wave relation*

It is interesting to note that an exact expression for the screech frequency can be obtained from the simple standing wave relation given in (2). Since $\lambda_s = c/f_s$ and $\lambda_h = u_c/f_s$ (where c is the ambient sound speed, f_s, is the screech frequency, and u_c is the convective speed of hydrodynamic fluctuations) (2) can be written as

$$\frac{1}{L_{sw}} = \frac{f_s}{c} + \frac{f_s}{u_c}.$$

Rearranging,

$$f_s = \frac{u_c}{L_{sw}(1 + u_c/c)}. \tag{3}$$

Equation (3) provides an exact expression, since it is derived from an exact kinematic relation without any approximations. An approximate expression is obtained if the wavelength of the standing wave is equated to the shock spacing, $L_{sw} \sim L$:

$$f_s = \frac{u_c}{L(1 + M_c)}, \tag{4}$$

where M_c is the convective Mach number, u_c/c. Equation (4) is identical to the relationship obtained by Powell (1953 *a*) from consideration of a feedback loop, and by Fisher & Morfey (1976) from consideration of the upstream directivity of a phased array of acoustic sources. Both models assume the existence of multiple line sources located shock spacing distances apart. A comparison between equations (3) and (4) shows that the correct choice is the standing wavelength. Also note that the exact expression can be arrived at using the same timing argument satisfied in a feedback loop (Powell 1953 *a*).

That the exact relation for the screech frequency does not require shock spacing is somewhat puzzling. After all screech only appears in a shock-containing jet; a correctly expanded jet does not screech. An exact answer to this issue has remained elusive. However, it is shown in the following section that the organized vortices responsible for the screech production are periodically modulated at the standing wavelength distance.

To complete the present discussion it will be shown that the screech frequency formula provided by Tam *et al.* (1986) can also be obtained from equation (3). Tam *et al.* assumes that the convective velocity of the hydrodynamic fluctuations is 70 % of that of the fully expanded jet velocity (u_j), i.e. $u_c = 0.7u_j$. Using isentropic relationships to relate u_j, and sound speed c, to the reservoir temperature T_r, ambient temperature T_a, and the fully expanded jet Mach number M_j, equation (3) can be written as

$$f_s = \frac{0.7u_j}{L_{sw}}\left[1 + 0.7M_j\left(1 + \frac{\gamma - 1}{2}M_j^2\right)^{-1/2}\left(\frac{T_r}{T_a}\right)^{1/2}\right]^{-1}. \tag{5}$$

For a circular jet, Tam *et al.* have used 80 % of the shock cell spacing to derive the empirical relation. Depending on the operating conditions, standing wave spacing can be smaller than, larger than or even equal to the shock spacing (Panda *et al.* 1997). Interestingly, table 1 shows that for the present experimental conditions, the standing wave spacing, L_{sw} is approximately 80 % of the average shock spacing. The

Prandtl–Pack formula (Pack 1950) provides the necessary relationship between the shock spacing and M_j:

$$L_{sw} \approx 0.8L = 0.8[1.306(M_j^2 - 1)^{1/2}D]. \tag{6}$$

Combining equations (5) and (6):

$$\frac{f_s D}{u_j} = \frac{0.67}{(M_j^2 - 1)^{1/2}} \left[1 + 0.7M_j \left(1 + \frac{\gamma - 1}{2} M_j^2\right)^{-1/2} \left(\frac{T_r}{T_a}\right)^{1/2}\right]^{-1}. \tag{7}$$

Equation (7) is the same as that of Tam *et al*., except for the minor replacement of fully expanded jet diameter, D_j, by the physical jet diameter D.

3.2.2. *Harmonic of the screech frequency*

Figure 6 shows fluctuating pressure levels close to the jet boundary, similar to figure 5, but for twice the screech frequency. To clarify the directivity patterns, equal-pressure contour levels are plotted for pressure fluctuations above 127 dB (figure 6*a*) and 140 dB (figure 6*b*). There are two distinct beams of sound, at 90° and about 120° to the jet axis. The angles are measured from the jet flow direction. The normal beam is stronger for the $M_j = 1.42$ jet (figure 6*b*) and the forward-propagating one is stronger for the $M_j = 1.19$ jet (figure 6*a*). An examination of the contour levels shows that the pressure amplitude decreases progressively away from the jet boundary. Once again, close to the jet boundary, there are indications of standing wave formation; however, the spacings are shorter and correspond to a linear superposition of harmonic-frequency waves. All of these show that the screech harmonic is primarily generated by the flow. Some additional support is found in the experimental data of Walker, Gordeyer & Thomas (1995) and Raman & Rice (1994), who have measured considerable velocity fluctuations at the harmonic frequencies inside the jet shear layer. The propagation nonlinearity of the fundamental tone has been suspected to be the cause of harmonic generation (Tam 1991). However, in view of the above discussion, the role of propagation nonlinearity may be relegated to a secondary status.

3.3. *Properties of organized structures*

Two properties of the organized structures are discussed in the following: convective velocity and coherent velocity fluctuations. The convective velocity of the organized vortices was measured directly inside the shear layer as well as indirectly through the hydrodynamic field, using two separate techniques. Both techniques involve measuring the relative phase (ϕ) between the time signals of a traversing probe, $R(x, t)$, and a fixed microphone, $P(t)$. The cross-correlation function between the two signals is first calculated and then the cross-spectral density function is determined. The phase value $\phi(x)$ of the cross-spectral density function measured at the screech frequency ($f = f_s$) is the desired relative phase (Panda *et al.* 1997). The calculations were performed directly through a frequency analyser (Spectral Dynamics) that provided an average phase over 128 K data points obtained over 6.4 s. Subsequently, the convective speed is obtained by evaluating the spatial derivative, $\mathrm{d}\phi(x)/\mathrm{d}x$, at each measurement station. The convective velocity u_c is normalized by the ambient sound speed c, and is expressed as a convective Mach number:

$$M_c = \frac{u_c}{c} = \frac{2\pi f_s}{(c\,\mathrm{d}\phi/\mathrm{d}x)}. \tag{8}$$

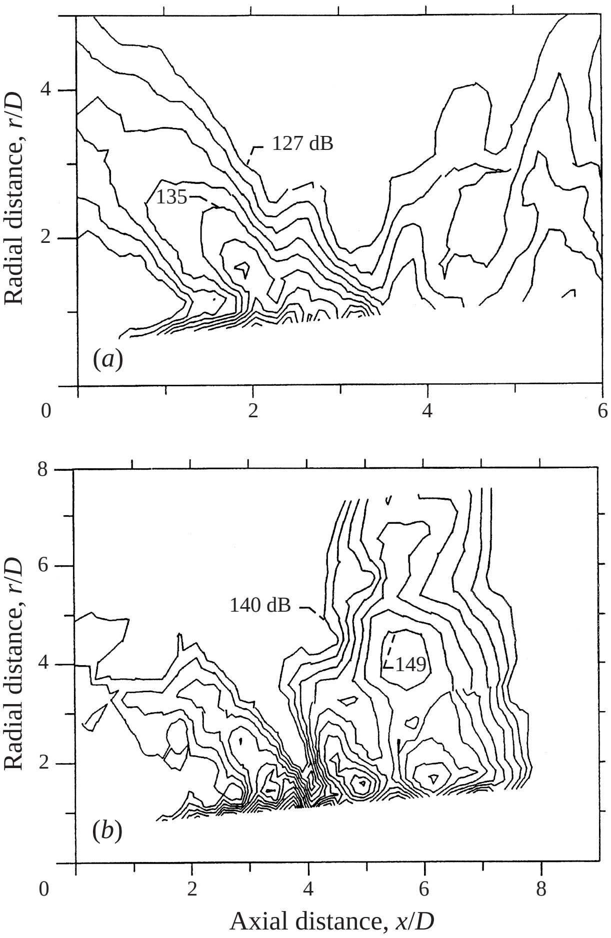

FIGURE 6. RMS pressure fluctuation at twice the screech frequency for (*a*) $M_j = 1.19$ and (*b*) 1.42 jets. The contour levels are at (*a*) 2 dB and (*b*) 1.5 dB intervals.

The derivative is calculated from the measured data using a compact three-point scheme (Anderson, Tennehill & Pletcher 1984).

3.3.1. *Convective velocity of coherent fluctuations inside shear layer*

The passage of the organized structures in the jet shear layer was detected by light scattering from a narrow laser beam passing perpendicular to the jet flow direction. The scattered light was sensed by a PMT as shown earlier in figure 2. The relative phase (ϕ) between the PMT signal and that of a fixed microphone was determined from cross-spectral analysis of the two signals. As the laser beam was moved from point to point the relative phase also changed, indicating a convection process. Figures 7(*a*) and 7(*c*) show the measured phase variation in the $M_j = 1.19$ and 1.42 jets along $r/D = 0.48$. Figures 7(*b*) and 7(*d*) show the corresponding convective velocity variation. Note that data points are omitted at axial stations where the laser beam interacts with a shock: since strong scattering by the shock waves completely overwhelms relatively weaker scattering by the organized structures, no phase measurements were possible at these stations. The average convective Mach

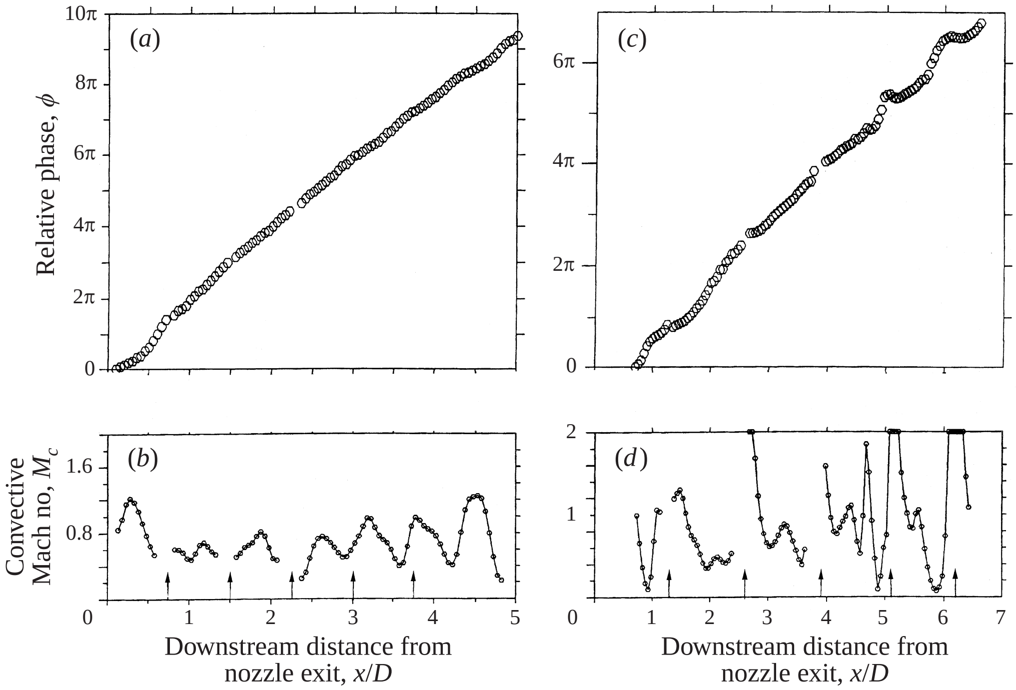

FIGURE 7. Phase and convective Mach number variations measured inside shear layer ($r/D = 0.48$) in (*a*), (*b*) $M_j = 1.42$ and (*c*), (*d*) 1.19 jets. Data obtained by laser light scattering from organized structures. The vertical arrows at the bottom of (*b*) and (*d*) represent shock locations.

number was calculated from a least-square straight line fit and is found to be 0.68 for the $M_j = 1.42$ jet and 0.7 for the $M_j = 1.19$ jet.

A careful examination of the phase variation data of figures 7(*a*) and 7(*c*) shows an underlying sinuous modulation superimposed on the general linear increase. Such a phase variation is indicative of a non-uniform convective speed which is plotted in figures 7(*b*) and 7(*d*) for respectively $M_j = 1.19$ and 1.42 jets. There is a relatively large error in the convective velocity calculation, particularly in the region where it is high supersonic. The problem lies with the derivative ($\mathrm{d}\phi/\mathrm{d}x$) calculation, which amplifies the random error in phase measurement. In spite of the measurement error, the large, periodic variation in the convective speed of the organized structures is very clear. Curiously the spatial periodicity matches with the standing wave spacing, not the shock spacing. From figures 7(*b*) and 7(*d*), the periodicity of variation is determined to be $0.68D$ and $1.07D$ for respectively $M_j = 1.19$ and 1.42 jets. A comparison with the various length scales provided in table 1 shows that, within the experimental accuracy, the above spatial periodicity is equal to the standing wave spacing. This result has a far-reaching implication, as it shows that the organized vortices are regularly modulated while passing over the shock train; the spatial periodicity, however, is that of the standing wavelength (not the shock spacing). In order to verify this observation a search was made of the literature. Hu & McLaughlin (1990) and Raman & Rice (1994) have measured convective velocity from the phase variation data as presented in figure 7. An examination of their phase data also reveals the same sinuous modulation as demonstrated in this paper. However, the

M_j	Screech frequency, f_s (Hz)	Convective Mach no., M_c	Expected standing wave spacing, L_{sw}/h	Average periodicity of u' modulation, $L_{u'}/h$	Average shock spacing, L/h^*
1.44†	7936	0.78	2.61	2.57	2.0
1.55‡	6336	0.78	3.24	3.17	2.5
2.1§	9450	1.02	1.9	2.0	1.5

* Normalizing parameter h represents the small nozzle dimension for a rectangular jet, and diameter for a circular jet.

† Raman & Rice (1994); rectangular jet.

‡ G. Raman, personal communication; rectangular jet.

§ Hu & McLaughlin (1990); circular jet.

TABLE 2. Length scales relevant to the modulation of turbulent fluctuations (u') in jet shear layer

associated phase speed variation, and the role of the standing wavelength were not noticed in the above references. Additional analysis of their data follows.

3.3.2. *Turbulent fluctuations in shear layer*

In the present programme no attempt was made to measure turbulent fluctuations. However, such data are available from prior experiments on underexpanded screeching jets by Hu & McLaughlin (1990) and Raman & Rice (1994). Hu & McLaughlin artificially excited their low-Reynolds-number underexpanded jet and performed phase-averaged measurements of mass–velocity fluctuation in the shear layer. Raman & Rice measured the axial component of velocity fluctuation in a high-Reynolds-number jet. In both experiments the turbulence fluctuation at the screech frequency was found to be modulated periodically. The spatial periodicity of the modulation (L_u) is calculated from their data, and is presented in table 2. From the measured data of screech frequency, and the average convective velocity, the expected standing wave spacing (L_{sw}) is also calculated. Within the experimental accuracy, the periodicity with which turbulent fluctuations are modulated is found to be the same as that of the standing wavelength.

3.3.3. *Convective speed of pressure fluctuations outside jet boundary*

Just outside the jet boundary the flow velocity is very small and a microphone can be placed to measure pressure fluctuation. The relative phase (ϕ) between a traversing and a fixed microphone was measured from the cross-spectral phase as indicated earlier. The fixed microphone was kept on the nozzle lip and the traversing microphone was moved from point to point along an oblique line just outside the shear layer. It was closest to the jet at the nozzle lip ($r/D = 0.6$ and 0.7 for respectively $M_j = 1.19$ and 1.42 jets) and was traversed at an angle of 5.71° to the jet axis. The phase and convective Mach number variation data are presented in figure 8 for both $M_j = 1.19$ and 1.42 jets. In addition, the root-mean-square of the fluctuating pressure (p_{rms}) at the screech frequency is also plotted (figure 8 *c*,*f*).

The microphone measurement has the advantage of providing data points even over the axial locations where shocks are present in the shear layer. The discontinuities in figure 7 are absent in figure 8. Nevertheless, the critical features are common to both. The convective speed is found to vary from a supersonic to subsonic value with a periodicity identical to that of the standing wave spacing. Noticeably, a minimum in the standing wave amplitude (figure 8 *c*,*f*) corresponds to a minimum in the convective velocity and vice versa.

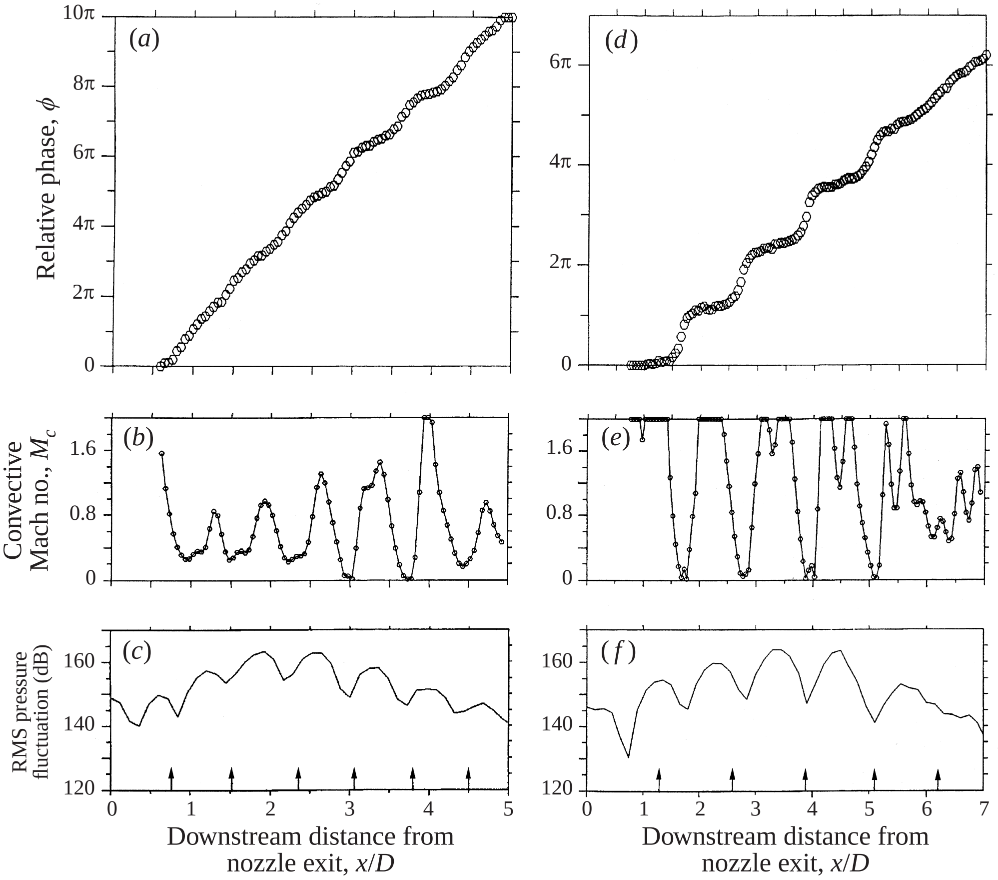

FIGURE 8. Phase, convective Mach number, and r.m.s. pressure fluctuations just outside the boundary of (*a*), (*b*), (*c*) $M_j = 1.42$, and (*d*), (*e*), (*f*) $M_j = 1.19$ jet. Relative phase values are from cross-spectra of a fixed and a traversing microphone signals. The vertical arrows in (*c*) and (*f*) are shock locations.

An explanation of the sinuous modulation lies in the partial interference caused by the oppositely moving hydrodynamic and acoustic fluctuations. It has been demonstrated by Wiegel & Wlezien (1993) and Panda *et al.* (1997) that when two oppositely moving wave systems produce a partial interference the phase and convective velocity modulates periodically as seen in figure 8. The hydrodynamic pressure field outside the jet flow boundary is strongly affected by the acoustic fluctuations; however, very close to the jet boundary hydrodynamic fluctuations overwhelm the acoustic contribution, and, therefore, the net fluctuation propagates downstream.

3.4. *Time evolution of near-field pressure fluctuations*

This section presents extremely detailed, unsteady pressure field data that ultimately show sound generation and propagation over a screech cycle. The phase-averaged pressure fluctuation measurements, shown in figure 9, were obtained over the same grid points as the time-averaged data. The signal from a microphone placed upstream of the nozzle was used as a reference for the phase-averaged measurements. To produce a repeatable phase reference, the reference microphone signal was bandpass filtered about the fundamental screech frequency. This eliminated the broadband noise components. (The same signal was also used for phase reference of the schlieren

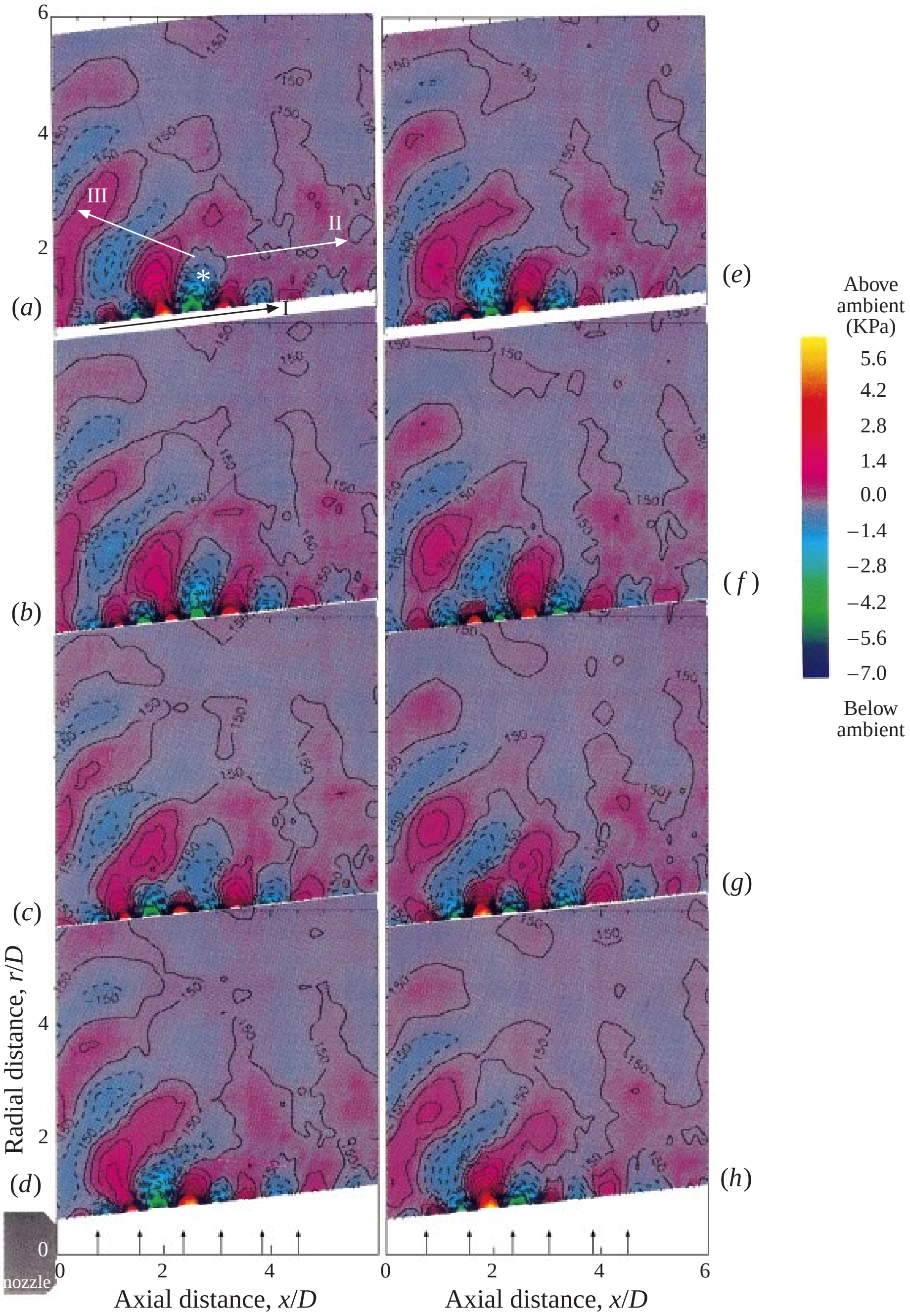

FIGURE 9. Phase-averaged fluctuating pressures, $\langle p \rangle$, for $M_j = 1.19$ jet. Phase time τ/T for (*a*)–(*h*): 0, 0.125, 0.25, 0.375, 0.5, 0.625, 0.75 and 0.875. The contour levels are at an interval of 150 Pa. Dashed contours represent below ambient and solid ones above ambient pressure. Arrow I shows the motion of hydrodynamic waves, and II and III that of acoustic waves. The vertical arrows at bottom represents shock locations.

photographs.) A 3.18 mm diameter microphone was traversed from point to point in the flow field and, at every measurement station the pressure signal, $p\{t, x/D, r/D\}$, was phase averaged over more than 100 screech cycles to obtain $\langle p\rangle\{\tau/T, x/D, r/D\}$. The data were stored in the Microvax computer for later processing.

A discussion on the measurement accuracy follows. The complete data set was repeated three times; twice using a 3.18 mm diameter microphone and once using a 6.35 mm diameter microphone. The pressure fluctuation values were found to be closely repeatable. The only major discrepancy appears in the absolute magnitude close to the jet boundary where a $\pm 5\,\%$ difference is not uncommon. This is not unexpected as the r.m.s. level along the jet boundary crosses the dynamic range of the microphone: 165 dB. The spatial resolution to which the pressure fluctuations can be resolved is not a problem except close to the jet boundary where a change of 20 dB can occur over a distance of $0.7D$ (17.8 mm, figure 5 *a*). The 3.18 mm diameter microphone introduces some spatial averaging over the area covered by the sensor diaphragm. The temporal resolution is limited by the sampling rate in the analogue-to-digital converter used to acquire the microphone signals. A sampling rate of $200\,000\ \mathrm{s}^{-1}$ and a screech frequency of 8400 Hz provided about 24 data points per cycle. This translates into a phase uncertainty of $\pm 8\,\%$. Another final concern that limits the measurement accuracy is the fluctuating plenum pressure which also changes the screech frequency. The compressed air was supplied from a central facility which feeds many other test installations. Therefore, a certain amount of fluctuation was unavoidable. However, the plenum pressure, measured using a Setra pressure transducer, was continuously monitored and the data acquisition was performed only when it remained within $\pm 0.5\,\%$ of the desired setting. The accompanying drift in screech frequency was ± 25 Hz. This condition was imposed for all data presented in this paper.

Each multi-colour plot of figure 9 shows a set of compression (above ambient, red-yellow) and rarefaction (below ambient, blue-green) regions which move in a complicated fashion as the phase time progresses. The instantaneous pressure levels at every measurement station are the resultant of hydrodynamic and acoustic fluctuations. It is impossible to isolate individual contributions as both are at the same frequency. Nevertheless, the advantage of working on a screeching jet is that the acoustic waves move primarily in the opposite direction to that of the organized vortices. Therefore, a careful examination of the propagation direction reveals many interesting features which can be attributed primarily to hydrodynamic or to acoustic waves. Note that in the commonly encountered mixing noise situation, both the acoustic and hydrodynamic fields propagate downstream and the advantage of separating the two is lost. An additional feature of the current data is that the measurement region covers more than eight shock cell spacings from the nozzle exit. It is known that sound sources lie within the fifth shock from the nozzle exit (Davis & Oldfield 1962). Therefore, the region covered by the experimental data should show not only a simple interaction between the hydrodynamic and the acoustic fluctuations but also the generation of the latter.

A complete wave is made of a compression and a rarefaction zone; therefore, a wavelength is the distance covered by two such adjacent zones. By following the motion of different such zones, from plot to plot, one can see the presence of two types of waves. The smaller wavelength ones lying next to the jet boundary, and having a high level of pressure fluctuations (green and deep red), are found to propagate downstream with the flow. Such waves are marked by the arrow I in figure 9 (*a*) and are identifiable within one radial distance from the bottom boundary of each colour plot. These are primarily associated with the hydrodynamic pressure fluctuation from large organized structures. The pressure maxima and minima associated with the hydrodynamic waves are very high. Some contour levels in such extreme regions close to the jet boundary are not drawn in figure 9 for the sake of clarity. The second type of waves occupy most of the measurement region. They have a larger wavelength, and are relatively weak (blue and pale red). They are present above the hydrodynamic waves and are found to propagate either upstream or downstream depending on their point of origin. These are identified primarily as the sound waves.

The nature of the hydrodynamic waves becomes particularly clear from a combined view of the flow field and the near-field pressure fluctuations. This is shown in figure 10 where the instantaneous pressure fluctuation data are superimposed on the phase-averaged schlieren photographs, obtained at identical phase times. The multi-colour pressure fluctuation plots are the same as shown in figure 9. The phase-averaged, multiple-exposure (six) schlieren photographs are somewhat similar to the single exposure ones shown earlier in figure 3. Like before, two trains of periodic dark patterns, the spatially fixed shock waves and the downstream-convecting organized turbulent eddies, are also visible in the schlieren photographs. The connection between the microphone data and the schlieren photographs is made through the hydrodynamic compression zones, which are manifested as darker regions beyond the jet boundary in the schlieren photographs, and the deep red regions along the lower boundary of the multi-colour plots. Since the phase-averaged microphone data and the schlieren photographs were obtained using identical trigger signals, phase matching was straightforward. Figure 10 demonstrates the radial penetration of hydrodynamic pressure fluctuations into the quiescent ambient air. It also confirms that the red-green regions, along the bottom boundary of each multi-colour plot, correspond to the hydrodynamic pressure fluctuations.

Returning to figure 9 (*a*), the propagation directions of the acoustic waves are shown by arrows II and III. The bases of the arrows lie in a demarcation region. All sound waves lying to the right of this region propagate downstream, while the rest propagate upstream. The blue-green rarefaction region that lies in the demarcation zone, and is marked by a star in figure 9 (*a*), shows a special behaviour not found elsewhere. The initial hydrodynamic fluctuations are found to produce a weaker rarefaction zone of length scale compatible to the acoustic wave. This is believed to be the beginning of an acoustic wave. The demarcation region lies nominally between the third and the fourth shock ($2.37 < x/D < 3.07$) and the development of the acoustic fluctuations occurs as the boundary of a compression or a rarefaction part of a passing hydrodynamic wave bulges out radially. A phase difference of half a cycle is maintained between the inception of the compression and the rarefaction part. In the following the development and growth of the rarefaction part alone is described.

The progressive development of the rarefaction zone, shown by a star in figure 9 (*a*), is traced in figure 11 where the same experimental data are plotted using the same contour levels, but without any colour. This figure provides a graphic demonstration of the interaction between multiple sources to produce a fully formed sound wave. The phase time of each plot of figure 11 is the same as that shown in figure 9. The only exceptions are figures 11 (*c*) and 11 (*i*). The former is added to make the sudden changes between 9 (*c*) and 9 (*d*) discernible and the latter to show the net change over a screech cycle. The rarefaction zone of figure 11 (*a*) is observed to bulge out radially, away from the jet boundary, to a size that corresponds to the half-wavelength of the screech waves (figure 11 *b*). It then shears off into two parts: the upper half, with a length scale corresponding to the sound wave, moves upstream

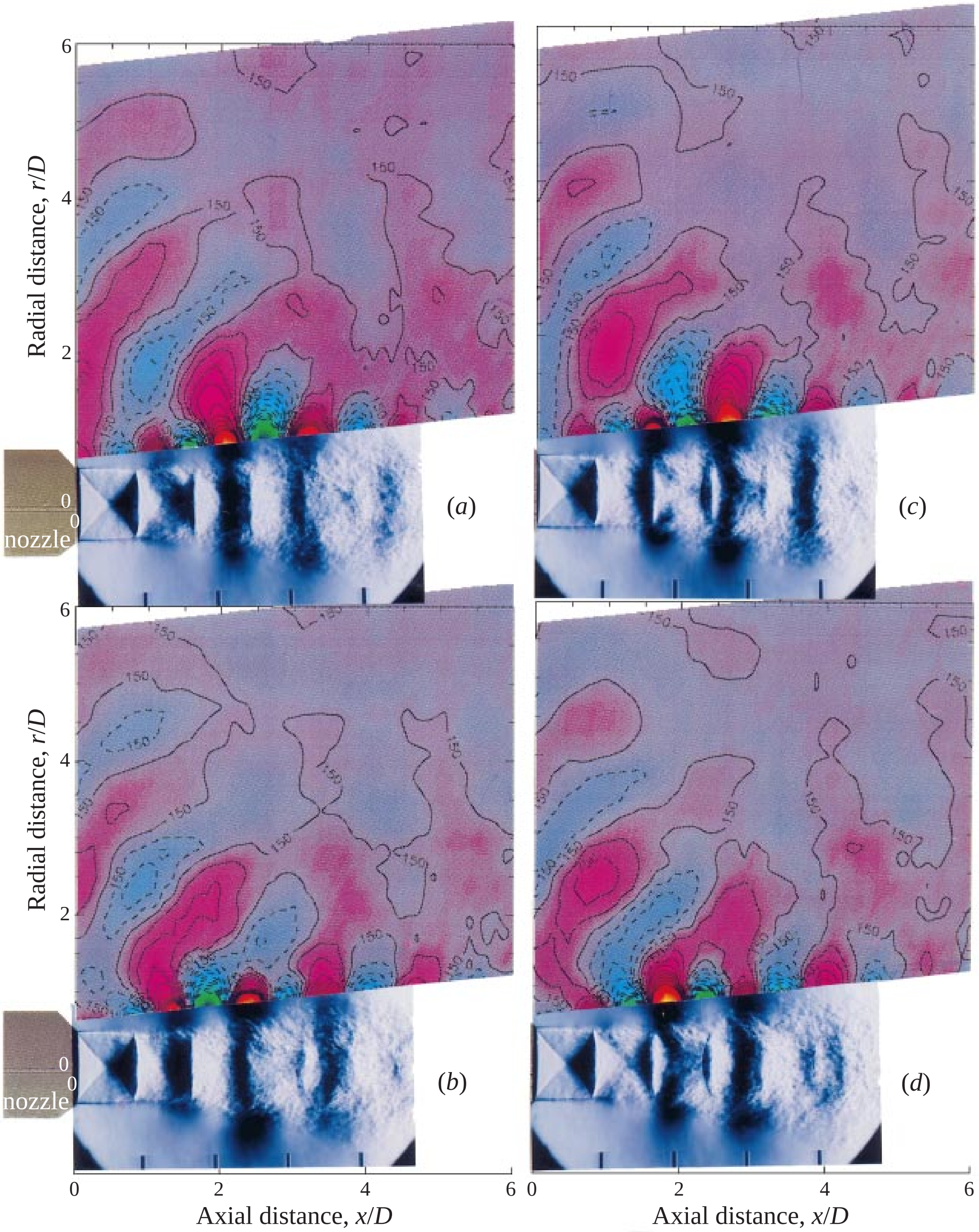

FIGURE 10. Phase-averaged schlieren photographs and fluctuating pressures, $\langle p \rangle$, at four different phases: (*a*) $\tau/T = 0$, (*b*) $= 0.25$, (*c*) $= 0.5$, (*d*) $= 0.75$, of screech cycle in $M_j = 1.19$ jet. The fluctuating pressure data are the same as in figure 9(*a*), (*c*), (*e*) and (*g*).

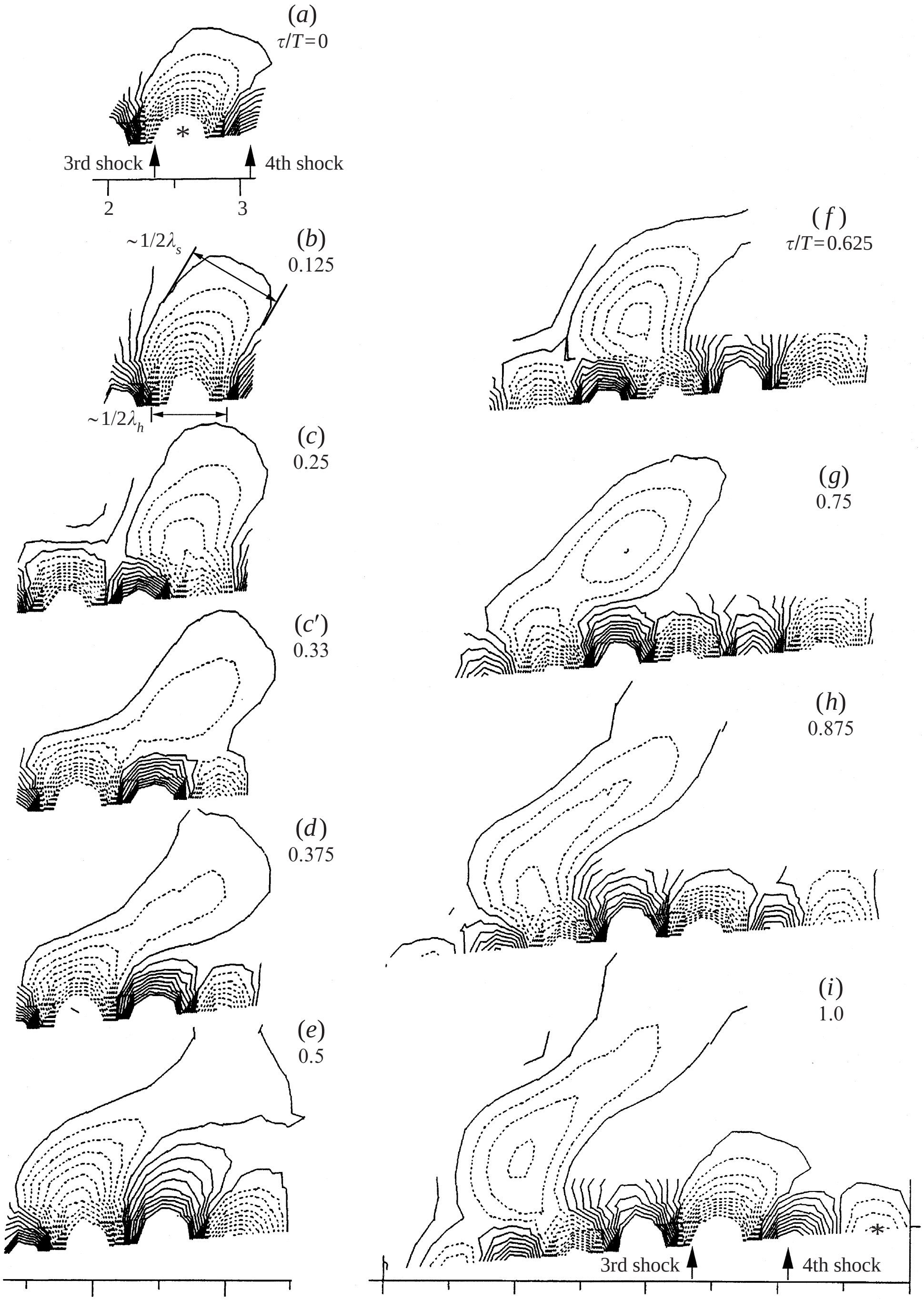

FIGURE 11. Selected regions of figure 9 are replotted to highlight the dynamics of one rarefaction region. The contour descriptions are also identical. Phase times τ/T are as indicated.

while the lower half, associated with the hydrodynamic field, continues its journey in the downstream direction. In between figures 11 (*c*) and 11 (*e*), the acoustic wave jumps over a dissimilar region associated with the hydrodynamic fluctuation and becomes attached to the similar region from the upcoming fluctuation. The process of repulsion between the dissimilar regions and attraction between the similar regions is performed two more times in the right half of figure 11. A video animation† of all data sets (24 frames covering a screech cycle) shows this motion very clearly. The compression or the rarefaction part of an acoustic wave is found to dwell on the similar part of a hydrodynamic wave for a relatively longer time and quickly jump over a dissimilar part. The resulting movement has a curious 'pause-and-go' feature that is very different from steady wave propagation. Such 'pause-and-go' feature and the amplitude modulation of the acoustic waves are telltale signs of a partially formed standing wave. It has been demonstrated by Panda *et al.* (1997) that the phase of a partially formed standing wave shows a spatially periodic modulation. The 'pause-and-go' feature is a result of this non-uniform phase variation.

Figure 11 (*i*) is at the same phase time as 11 (*a*); the only difference is that a complete screech cycle has passed in between. The original rarefaction part of the hydrodynamic wave has moved downstream to a location shown by a star, while a fully formed acoustic wave is approaching the nozzle exit. Notice that a new acoustic wave is developing between the third and fourth shock. Clearly, the fully formed acoustic wave is far stronger than the one at inception. The required energy transfer from the hydrodynamic to the acoustic wave has occurred during the interaction processes depicted between figures 11 (*b*) and 11 (*h*). A closer examination of the changes in the contour levels reveals that the rarefaction part of a sound wave becomes slightly weaker when passing over a dissimilar region of a hydrodynamic fluctuation; however, the loss is more than compensated for when similar regions of the acoustic and the hydrodynamic fluctuations interact. Therefore, various parts of the hydrodynamic field act as multiple sources that cause origination as well as nurturing of a sound wave.

Figure 11 describes the dynamics of the rarefaction part of a sound wave. The complementary compression part also develops between the third and the fourth shocks in figure 9 (*e*) and can be found to follow the same dynamics described above. An additional set of data showing the sound generation and propagation process for the $M_j = 1.42$ jet was acquired. The video tape, mentioned earlier, contains an animation of this data set. The fundamental dynamics of the acoustic and the hydrodynamic waves are found to be the same as described above.

4. Summary and conclusion

An experimental investigation of the intricate dynamics that lead to screech noise generation and propagation is presented in this paper. The detailed unsteady data resolved with high temporal resolution at well-defined phases of the screech cycle, and additional coupling with the flow visualization pictures, provide a more thorough description than any previous study. A preliminary analysis of the experimental data is found to produce some new observations. The following is a summary of the new observations, and a discussion of various unresolved issues at hand.

The plume of an underexpanded jet is characterized by a periodic shock train.

---

† The video animation titled, 'Pressure wave propagation in a screech cycle', is available from the NASA Center for AeroSpace Information, 800 Elkridge Landing Road, Linthicum Heights, MD 21090-2934, USA, under NASA CR-198467.

Traditionally, the average shock spacing is thought to be the primary length scale governing the screech phenomenon. A major contribution of this paper is in demonstrating the importance of a new length scale, the standing wavelength, in the sound generation process. The new length scale is called the ‘standing wavelength’ because it is found to be equal to the distance between the node points in the interference pattern formed by the hydrodynamic and acoustic fluctuations.

In a screeching jet, large organized vortices interact with the periodic shock train to create the screech sound. Spark schlieren photographs presented here demonstrate this feature nicely. The convective velocity of the organized vortices is measured using a non-intrusive, line-of-sight laser scattering technique. It is observed that the convective velocity is periodically modulated inside the jet shear layer. The turbulent fluctuation data obtained by Hu & McLaughlin (1990) and Raman & Rice (1994) also show the same trend. Interestingly, it is found that the spatial periodicity of modulation does not follow the shock spacing; it is equal to the new length scale represented by the ‘standing wavelength’. The latter is close to yet different from the average shock spacing. The reason for the difference cannot be explained.

The periodically modulated organized vortices are also found to be the germination and nurturing bed of the screech sound waves. The potential pressure field (also called the hydrodynamic field) of the organized vortices extends outside the jet boundary and is found to create an interference with the germinating sound waves. The root-mean-square pressure fluctuation measured in the immediate vicinity of the jet boundary clearly demonstrate the interference as a standing wave pattern. The interference is incomplete; depending on the radial distance from the jet boundary either the hydrodynamic or the acoustic fluctuations dominate. To reveal the mechanism of sound wave generation individual compression and rarefaction parts are traced through a detailed phase-averaged pressure fluctuation survey. Such surveys are made in the near field of the $M_j = 1.19$ and 1.42 jets. A description of the dynamics, using additional information from the phase-matched schlieren photographs, is provided in the text. A video animation of the unsteady data further illustrates the description. The sound waves are found to propagate in a curious ‘pause-and-go’ motion along the jet boundary, where the individual compression and rarefaction parts of an acoustic wave are found to dwell on the similar parts of an hydrodynamic wave for a relatively longer time and quickly jump over a dissimilar part. Such behaviour, once again, is attributed to the partial interference effect. The harmonic frequency sound waves are also found to be generated from the same frequency organized vortices present inside the shear layer.

An exact expression for the screech frequency is found from the standing wave relationship. The existing screech frequency formulations, due to Powell (1953), Fisher & Morfey (1976) and Tam *et al.* (1986), are known to provide only an approximate match with the experimental data. The primary difference between the existing models and the exact expression is a replacement of the average shock spacing by the standing wave spacing.

An important query, that has remained unanswered, is the reason for the organized vortices to modulate at the standing wave spacing, instead of the shock spacing, while convecting over the shock train. The feedback loop apparently chooses the new length scale represented by the standing wavelength in selecting the screech frequency. Perhaps detailed flow-field measurements and an analysis of the shock–vortex interaction will be helpful in resolving this issue.

The author acknowledges help in setting up the schlieren system from Ken E. Weiland and Carolyn R. Mercer of NASA Lewis.

REFERENCES

Anderson, D. A., Tennehill, J. C. & Pletcher, R. H. 1984 *Computational Fluid Dynamics*. McGraw-Hill.

Brocher, E. & Makhsud, A. 1997 A new look at the screech tone mechanism of underexpanded jets. *Eur. J. Mech.* B/*Fluids* **16**, 877–891.

Cain, A. B., Bower, W. W., Walker, S. H. & Lockwood, M. K. 1995 Modeling supersonic jet screech Part 1: vortical instability wave modeling. *AIAA Paper* 95-0506.

Dahl, M. D. 1994 The aeroacoustics of supersonic coaxial jets. PhD dissertation, The Pennsylvania State University. Also *NASA TM* 106782.

Davis, M. G. & Oldfield, D. E. S. 1962 Tones from a chocked axisymmetric jet. I. Cell structure, eddy velocity and source locations. *Acustica* **12**, 257–277.

Fisher, M. J. & Morfey, C. L. 1976 Jet noise. *AGARD Lecture Series* 80, Aerodynamic Noise.

Hay, J. A. & Rose, E. G. 1970 In flight shock cell noise. *J. Sound Vib.* **11**, 411–420.

Hu, T. F. & McLaughlin, D. K. 1990 Flow and acoustic properties of low mach number underexpanded supersonic jet. *J. Sound Vib.* **141**, 485–505.

Morris, P. J. 1977 Flow characteristics of the large scale wavelike structure of a supersonic round jet. *J. Sound Vib.* **53**, 223–244.

Norum, T. D. & Seiner, J. M. 1980 Location and propagation of shock associated noise from supersonic jets. *AIAA Paper* 80-0983.

Pack, D. C. 1950 A note on Prandtl's formula for the wavelength of a supersonic gas jet. *Q. J. Mech. Appl. Maths* **III**, 173–181.

Panda, J. 1995*a* Measurement of shock oscillation in underexpanded supersonic jets. *AIAA Paper* 95-2145.

Panda, J. 1995*b* A shock detection technique based on light scattering by shock. *AIAA J.* **33**, 2431–2433.

Panda, J. 1998 Shock oscillation in underexpanded supersonic jets. *J. Fluid Mech.* **363**, 173–198.

Panda, J., Raman, G. & Zaman, K. B. M. Q. 1997 Underexpanded screeching jets from circular, rectangular and elliptic nozzles. *AIAA Paper* 97-1623.

Poldervaart, L. J., Vink, A. T. & Wijnands, A. P. J. 1968 The photographic evidence of the feedback loop of a two dimensional screeching supersonic jet of air. *6th Intl Congr. on Acoustics, Tokyo, Japan*, pp. 21–28.

Powell, A. 1953*a* On the noise emanating from a two-dimensional jet above the critical pressure. *Aeronaut. Q.* **IV**, 103–122.

Powell, A. 1953*b* On the mechanism of choked jet noise. *Proc. Phys. Soc.* (*Lond.*) **66**, 1039–1056.

Raman, G., Panda, J. & Zaman, K. B. M. Q. 1997 Feedback and receptivity during jet screech: influence of an upstream reflector. *AIAA Paper* 97-0144.

Raman, G. & Rice, E. J. 1994 Instability modes excited by natural screech tones in a supersonic rectangular jet. *Phys. Fluids* **6**, 3999–4008.

Rice, E. J. & Taghavi, R. 1992 Screech noise source structures of a supersonic rectangular jet. *AIAA Paper* 92-0503.

Seiner, J. M., Manning, J. C. & Ponton, M. K. 1987 Model and full scale study of twin supersonic plume resonance. *AIAA Paper* 87-0244.

Strohben, J. W. (Ed.) 1978 *Laser Beam Propagation in the Atmosphere*. Springer.

Tam, C. K. W. 1991 Jet noise generated by large-scale coherent motion. In *Aeroacoustics of Flight Vehicles: Theory and Practice, Vol. 1: Noise Sources* (ed. H. H. Hubbard), pp. 311–390. *NASA RP*-1258, WRDC TR-90-3052.

Tam, C. K. W., Ahuja, K. K. & Jones, R. R. 1994 Screech tones from free and ducted supersonic jets. *AIAA J.* **32**, 917–922.

Tam, C. K. W., Seiner, J. M. & Yu, J. C. 1986 Proposed relationship between broadband shock associated noise and screech tones. *J. Sound Vib.* **110**, 309–321.

Truman, C. R. 1992 The influence of turbulent structures on optical phase distortion through turbulent shear flows. *AIAA Technology Conf.*

Walker, W. H., Gordeyev, S. V. & Thomas, F. O. 1995 A wavelet analysis applied to unsteady jet screech resonance. *ASME Fluids Engng Conf., Forum on High Speed Jets.*

Westley, R. & Woolley, J. H. 1968 An investigation of the near noise fields of a choked axisymmetric air jet. In *Aerodynamic Noise* (ed. H. S. Ribner), pp. 147–167. University of Toronto Press.

Westley, R. & Woolley, J. H. 1969 The near field sound pressures of a choked jet during a screech cycle. In *Aircraft Engine Noise and Sonic Boom,* Paper 23. *AGARD CP*-42.

Westley, R. & Woolley, J. H. 1970 Shock cell noise-mechanisms, the near field sound pressure associated with a spinning screech mode. *Conf. on Current Developments in Sonic Fatigue, Institute of Sound and Vibration Research, University of Southampton.*

Wiegel, M. & Wlezien, R. W. 1993 Acoustic receptivity of laminar boundary layers over wavy walls. *AIAA Paper* 93-3280.

Yu, J. C. & Seiner, J. M. 1983 Nearfield observations of tones generated from supersonic jet flows. *AIAA Paper* 83-0706.